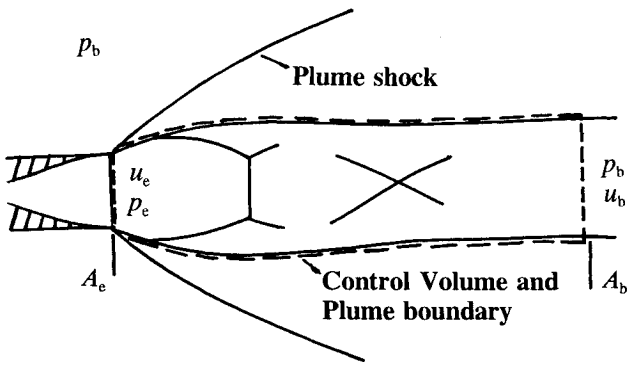

Fig. 1 Control volume analysis of a low-altitude plume.

The integral in Eq. (1) is the axial force applied by the free-stream and is termed the plume drag, D. Pearce and Dash, following Sukanek, estimated its magnitude from Jarvinen and Hill's universal plume model[2] for which

$$\frac{D}{F} = \left(\frac{C_{F_{\max}}}{C_F}\right) - 1 = \frac{F_{\max} - F}{F} \tag{2}$$

For this model it can be seen that D is independent of the rocket's speed and largely determined by the exit Mach number of the rocket nozzle. The model has been applied successfully to the estimation of plume size and shape but the drag dependence is weak (quarter power) for that problem.[3] Its application to the matched pressure problem is examined subsequently.

The maximum thrust $F_{\max}$ that a rocket engine can produce is equal to the maximum momentum that it can impart to the exhaust gas, and thus the maximum thrust coefficient is normally defined as

$$C_{F_{\max}} = \dot{m}u_\infty / p_c A^* \tag{3}$$

For a gas with a constant ratio of specific heats this can be written

$$C_{F_{\max}} = \left\{\frac{2\gamma^2}{\gamma - 1}\left(\frac{2}{\gamma + 1}\right)^{(\gamma+1)/(\gamma-1)}\right\}^{1/2} \tag{4}$$

This is the definition of $C_{F_{\max}}$ used in the universal plume model.[1] However, in their application of the model, Pearce and Dash redefined $C_{F_{\max}}$ as

$$C_{F_{\max}} = \left\{\frac{2\gamma^2}{\gamma - 1}\left(\frac{2}{\gamma + 1}\right)^{(\gamma+1)/(\gamma-1)}\left[1 - \left(\frac{p_b}{p_c}\right)^{(\gamma-1)/\gamma}\right]\right\}^{1/2} \tag{5}$$

The extra factor is equivalent to u/u_∞, where u is the velocity obtained in an isentropic expansion to p_b (with constant γ). Therefore, Pearce and Dash have not used the universal plume model but have effectively assumed that the plume drag is just sufficient to allow an isentropic expansion of the exhaust gas to the ambient pressure. This draws attention to the second inconsistency in their paper, because in their Fig. 1, Pearce and Dash show a difference between plume temperature calculated with the "corrected theory" and that calculated assuming an isentropic expansion. The two approaches are identical and the difference in result arises from the assumption of constant γ in the corrected theory and the use of a set of nozzle exit and stagnation conditions which are not consistent with constant γ. The plume flowfield and rocket thrust are of course determined by the nozzle exit conditions regardless of what processes took place in the expansion up to that point. However, if one refers to the conditions in the combustion chamber when calculating the rocket thrust then the nature of the expansion in the nozzle must be taken into account. Pearce and Dash failed to do so and produced a spurious result for the plume temperature which quite coincidentally agreed with their numerical calculation.

Conclusion

When the universal plume model is used correctly to estimate the plume drag so that the temperature in the matched pressure plume can be calculated, the rather uninteresting result is $T_b = 0$ K. The example application presented by Pearce and Dash (their Fig. 1) shows that the self-consistent simple model of an isentropic expansion from p_e to p_b gave results not too far removed from the numerical calculations. It may be possible to improve the isentropic model slightly by adding some fraction of the total possible isenthalpic entropy increase, $R\ell_n(p_c/p_b)$. However, given the sensitivity of the infrared emission to the plume temperature, it may be that only a full numerical simulation will give sufficiently accurate results.

References

[1]Sukanek, P. C., "Matched Pressure Properties of Low Altitude Plumes," *AIAA Journal*, Vol. 15, No. 12, 1977, pp. 1818–1821.

[2]Pearce, B. E., and Dash, S. M., "Use of Matched Pressure Initial Conditions for Predicting Low-Altitude Rocket Plume Radiation," *AIAA Journal*, Vol. 17, No. 6, 1979, pp. 667–670.

[3]Draper, J. S., and Sutton, E. A., "A Nomogram for High-Altitude Plume Structures," *Journal of Spacecraft and Rockets*, Vol. 10, No. 10, 1973, pp. 683, 684.

Analysis of Interlaminar Stresses in the Torsion of Symmetric Laminates

James M. Whitney*
University of Dayton, Dayton, Ohio 45469

Introduction

In a recent paper[1] a modified shear deformation theory (SDT) based on Reissner-type assumptions[2] was considered in obtaining an approximate solution for the torsion of a symmetrically laminated, anisotropic plate. In-plane stresses were modified to satisfy free-edge boundary conditions. Interlaminar stresses were obtained by integrating the equations of equilibrium. Thus, the resulting stresses satisfied point-by-point equilibrium as well as the correct boundary conditions.

This same procedure has also been applied to the case of a $[0/90\ \text{deg}]_s$ laminate under uniaxial tension loading.[3] However, numerical results indicate that the maximum value of the interlaminar normal stress, σ_3, at the the laminate midplane underestimates the value obtained from theory of elasticity. In addition, the distance away from the free edge over which the interlaminar normal stress dissipates was greater than that obtained from the elasticity solution.

These discrepancies are attributed to the vanishing of the interlaminar normal strain component associated with the modified shear deformation theory. This conclusion is supported by the work of Pagano.[4] In particular, he obtained excellent results for the distribution of σ_3 at the midplane of a $[0/90\ \text{deg}]_s$ laminate by utilizing a shear deformation theory in conjunction with a thickness-stretch mode (linear transverse displacement through the thickness). His procedure involved treating the upper half of the composite as a laminated plate with the distribution of σ_3 at the midplane being an unknown function. Although this approach produced excellent results for the distribution of σ_3 at the midplane, it did not provide for an accurate calculation of σ_3 through

Received Feb. 5, 1993; presented as Paper 93-1507 at the AIAA/ASME/ASCE/AHS/ASC 34th Structures, Structural Dynamics, and Materials Conference, La Jolla, CA, April 19–21, 1993; revision received Sept. 16, 1993; accepted for pubication Sept. 20, 1993.

*Professor, Graduate Materials Engineering. Associate Fellow AIAA.

the thickness. This is discussed in detail by Pagano in his monograph.[5]

In the present paper the effect of transverse (interlaminar) normal strain on the torsional response of symmetrically laminated, anisotropic plates is investigated. The analysis is based on a modified form of the global laminate model developed by Pagano and Soni.[6] In-plane stresses are modified in the boundary zone to satisfy free-edge boundary conditions. For the general case of angle-ply layers, a laminated composite behaves in a manner similar to an anisotropic plate. The existence of the bending-twisting coupling phenomenon found in the case of anisotropic plates leads to two classic problems in conjunction with torsional loading. In the first case, referred to as "pure torsion," the torsional axis of the plated does not bend. Thus, an axial bending moment is required in addition to the torsional load to suppress plate bending. In the second case, referred to as "free torsion," the only loading is torque in which anisotropy induces bending of the torsional axis. For the purposes of this paper it is sufficient to consider the case of pure torsion only.

Analysis

We consider a rectangular plate with a conventional x, y, z coordinate system located in the midplane. The plate thickness and in-plane dimensions are denoted by h, a, and b, respectively. In addition, the plate is constructed of an arbitrary number of layers with a symmetric stacking sequence.

For the case of a symmetrically laminated, anisotropic plate subjected to torsion, we appy the global laminate model[6] that is based on the displacement field

$$u = z\psi_x(x, y), \qquad v = z\psi_y(x, y)$$
$$w = w(x, y) + z\psi_z(x, y) + \frac{z^2}{2}\phi(x, y) \tag{1}$$

where u, v, and w are displacements in the x, y, and z directions, respectively. These displacements contain transverse shear deformation in a classical manner while adding transverse normal strain effects by assuming w to be quadratic in the z coordinate. In the case of torsional loading, the absence of any surface tractions leads to the vanishing of ψ_z.

At this point we introduce a modification to the original theory by assuming that the transverse normal stress σ_3 has little effect on the in-plane stresses, i.e., we assume ply constitutive relations of the form

$$\sigma_i = Q_{ij}\varepsilon_j \qquad (i, j = 1, 2, 6)$$
$$\sigma_3 = C_{3m}\varepsilon_m \qquad (m = 1, 2, 3, 6) \tag{2}$$
$$\sigma_k = C_{kn}\varepsilon_n \qquad (k, n = 4, 5)$$

where the various C and Q are the anistropic stiffnesses and reduced stiffnesses for plane stress, respectively. This assures that a plane stress exact elasticity solution is recovered outside of the free-edge zone where the interlaminar stresses vanish.

For pure torsion about the x axis the solution for the in-plane stresses is of the form[7]

$$\sigma_i^{(k)} = zQ_{ij}^{(k)}\bar{D}_{j6}M_6\langle{}^{i\,=\,1,2,6}_{j\,=\,2,6}\rangle \tag{3}$$

where

$$\bar{D}_{j6} = \frac{(D_{j6}^*D_{11}^* - D_{1j}^*D_{16}^*)}{D_{11}^*}$$

and D_{ij}^* are elements of the inverse of the D_{ij} bending stiffness matrix. In addition, the twisting moment M_6 is given by the relationship

$$M_6 = -\frac{2\beta}{\bar{D}_{66}}\left[1 - \frac{1}{D}\left(L_2\lambda_2 \sinh\frac{\lambda_2}{2}\cosh\lambda_1\frac{y}{b} - L_1\lambda_1\sinh\frac{\lambda_1}{2}\cosh\lambda_2\frac{y}{b}\right)\right]$$

where

$$D = L_2\lambda_2\cosh\frac{\lambda_1}{2}\sinh\frac{\lambda_2}{2} - L_1\lambda_1\sinh\frac{\lambda_1}{2}\cosh\frac{\lambda_2}{2}$$

and where L_i and λ_i are functions of plate stiffness coefficients.[7]

Interlaminar Stresses

Interlaminar shear stresses for the kth layer can be determined from the equilibrium equations of elasticity. Thus,

$$\sigma_4^{(k)} = -\int_{-h/2}^{z^{(k)}}\sigma_{2,y}^{(k)}\,dz, \qquad \sigma_5^{(k)} = -\int_{-h/2}^{z^{(k)}}\sigma_{6,y}^{(k)}\,dz$$
$$\sigma_3^{(k)} = -\int_{-h/2}^{z^{(k)}}\sigma_{4,y}^{(k)}\,dz \tag{4}$$

The accuracy of Eqs. (4) depends on the following boundary conditions being exactly satisfied:

$$\sigma_i^{(k)}(\pm b/2) = 0 \qquad (i = 2, 4, 6) \tag{5}$$

In the case of pure torsion , the in-plane stresses $\sigma_2^{(k)}$ and $\sigma_6^{(k)}$ do vanish on the boundary, whereas $\sigma_4^{(k)} \neq 0$ on the free edge.

The in-plane stress $\sigma_2^{(k)}$, as given by Eq. (3), is modified as follows:

$$\sigma_2^{(k)} = zQ_{2j}^{(k)}\bar{D}_{j6}[M_6(y) + f(y)] \qquad (j = 2, 6) \tag{6}$$

where

$$f(y) = \frac{2}{D}\left(\frac{y}{b}\right)\left(A\sinh\lambda_1\frac{y}{b} + B\sinh\lambda_2\frac{y}{b}\right)$$

The values of A and B are determined from the conditions

$$f(\pm b/2) = \left[M_6'(\pm b/2) + f'(\pm b/2)\right] = 0 \tag{7}$$

The first condition assures that $\sigma_2^{(k)}$ remains zero at the boundary. A cursory examination of the interlaminar equilibrium relations, Eqs. (4), reveals that the second relationship in Eq. (7) is necessary to assure the vanishing of $\sigma_4^{(k)}$ on the boundary. Combining Eqs. (6) and (7), we obtain the unknown coefficients

$$A = \frac{(L_2 - L_1)\lambda_1\lambda_2\sinh(\lambda_1/2)\sinh^2(\lambda_2/2)}{D_m}$$
$$B = \frac{(L_1 - L_2)\lambda_1\lambda_2\sinh^2(\lambda_1/2)\sinh(\lambda_2/2)}{D_m} \tag{8}$$

where

$$D_m = \lambda_1\cosh\frac{\lambda_1}{2}\sinh\frac{\lambda_2}{2} - \lambda_2\sinh\frac{\lambda_1}{2}\cosh\frac{\lambda_2}{2}$$

It should be noted that these modified functions maintain the original symmetry of $\sigma_2^{(k)}$ relative to the y coordinate. This proce-

dure assures that equilibrium is satisfied point by point throughout the plate. However, compatibility in the boundary region will not be satisfied.

Numerical Results and Discussion

Numerical results are now considered using the following unidirectional ply properties:

$$\frac{E_L}{E_T} = 16, \quad \frac{E_3}{E_T} = 1, \quad \frac{G_{LT}}{E_T} = \frac{G_{L3}}{E_T} = 0.615$$

$$\frac{G_{T3}}{E_T} = 0.323, \quad \nu_{LT} = \nu_{L3} = 0.3, \quad \nu_{T3} = 0.55 \tag{9}$$

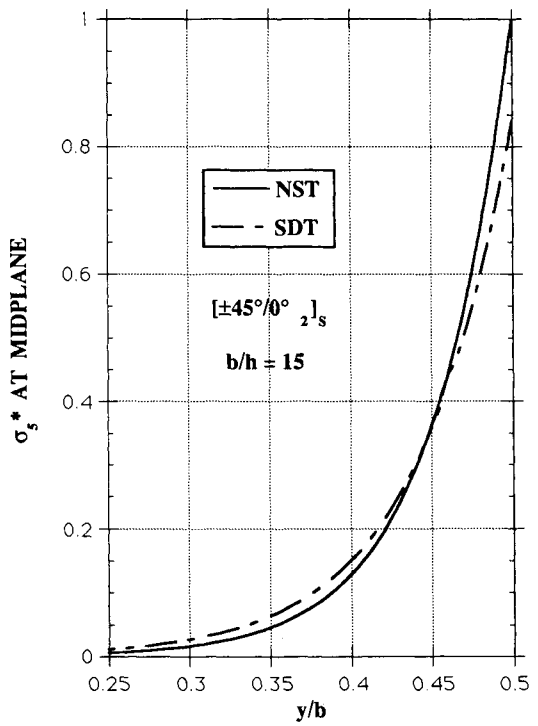

Fig. 1 Free-edge zone distribution of σ_5.

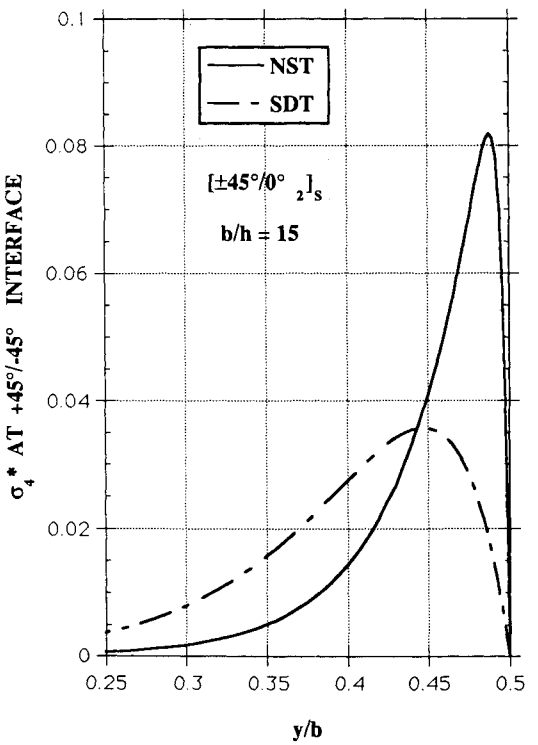

Fig. 2 Free-edge zone distribution of σ_4.

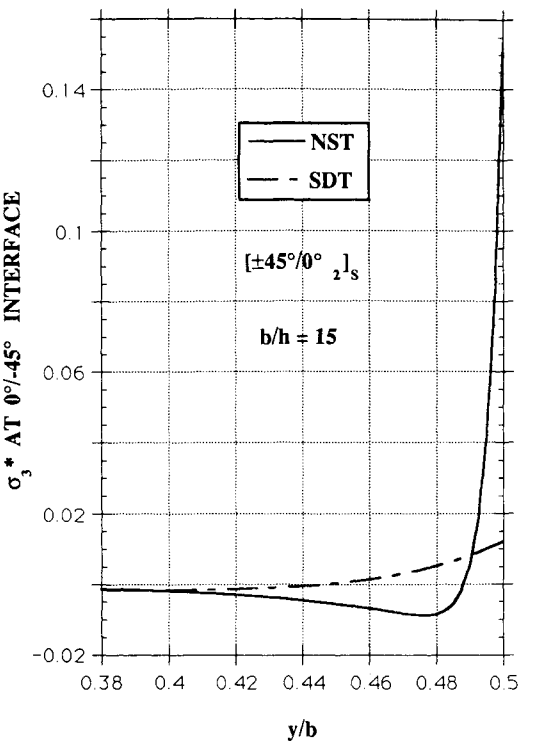

Fig. 3 Free-edge zone distribution of σ_3.

where the subscripts L, T, and 3 denote axes parallel to the fiber, perpendicular to the fiber, and through the thickness of a unidirectional composite, respectively. In addition E_i, G_{ij}, and ν_{ij} denote the Young's modulus in the ith direction, the shear modulus relative to the i-j plane, and the Poisson's ratio measured by contraction in the jth direction during a uniaxial tensile test in the ith direction, respectively.

Distribution of interlaminar stresses in the free-edge zone are shown in Figs. 1–3 for a $[\pm 45/0_2]s$ laminate with a width-to-thickness ratio $b/h = 15$. A comparison is made between the current normal strain (NST) theory and shear deformation (SDT) theory. All stresses are normalized by the maximum value of σ_5, which occurs at the free edge of the laminate midplane. The interlaminar stresses shown in Figs. 2 and 3 have been modified in accordance with Eq. (6). A similar type of modification, as discussed in Ref. 7, has been performed in conjunction with the SDT solutions.

Results in Figs. 1–3 illustrate that the effect of transverse normal strain is to stiffen the laminate. In particular, NST leads to larger interlaminar stresses compared with SDT. In Fig. 1 we see a slight increase in σ_5 near the boundary for NST compared with SDT. For the interlaminar stresses shown in Figs. 2 and 3, considerable increase is noted for the NST solution compared with SDT. Of particular note in Fig. 3, in addition to the rather dramatic increase in the NST solution compared with SDT, is the rapidity with which the present solution for σ_3 dissipates away from the boundary. This behavior has been previously noted for uniaxial in-plane loading of $[0/90]s$ laminates.[4]

References

[1]Whitney, J. M., "Analysis of Laminated, Anisotropic Plates Subjected to Torsional Loading," *Composites Engineering*, Vol. 3, No. 6, 1993, pp. 567–582.

[2]Reissner, E., "A Consistent Treatment of Transverse Shear Deformations in Laminated Anisotropic Plates," *AIAA Journal*, Vol. 10, No. 5, 1972, pp. 716–718.

[3]Whitney, J. M., "Approximate Free-Edge Stresses in an Orthotropic Laminated Composite Under Uniaxial Inplane Loading," *Proceedings of Advanced Composites 93*, The Metallurgical Society, Warrendale, PA, 1993, pp. 343–349.

[4]Pagano, N. J., "On the Calculation of Interlaminar Normal Stress in Composite Laminates," *Journal of Composite Materials*, Vol. 8, Jan. 1974, pp. 65–77.

[5]Pagano, N. J., "Models for Studying Free-Edge Effects," *Interlaminar Response of Composite Materials*, Vol. 5, Composite Materials Series, edited by N. J. Pagano, Elsevier, London, 1989, pp. 17–23.

[6]Pagano, N. J., and Soni, S. R., "Global-Local Laminate Variational Model," *International Journal of Solids and Structures*, Vol. 19, No. 3, 1983, pp. 207–228.

[7]Whitney, J. M., "The Effect of Transverse Normal Strain on the Torsion of Laminated Anisotropic Plates," *Proceedings of the AIAA/ASME/ASCE/AHS/ASC 34th Structures, Structural Dynamics, and Materials Conference*, Pt. 3, AIAA, Washington, DC, 1993, pp. 1732–1739.

Influence of Clamp-Up Force on the Strength of Bolted Composite Joints

Walter J. Horn*
Wichita State University, Wichita, Kansas 67260
and
Ron R. Schmitt†
Boeing Company, Wichita, Kansas 67277

Introduction

COMPOSITE materials offer the potential for a reduction in the number of individual parts and joints in a structure because large one-piece components can replace multipart assemblies. Nevertheless, there are many situations where composite parts must be joined and often mechanical fasteners provide the only practical method of joining those parts. The long-term strength of mechanically fastened joints of composite members can be directly affected by the clamp-up force of the fastener and thus perhaps by the relaxation of this force due to the viscoelastic character of the composite materials of the joint.

Collings[1] provided a comparison of the behavior of composite joints with pins with no lateral constraint, finger-tight lateral constraint, and high lateral constraint. Stacking sequence and fiber orientation were shown to affect the bearing strength for the three constraint conditions considered. Experimental results by Crews[2] for graphite/epoxy laminates indicated that increasing fastener clamp-up force in a joint improved both the static strength and fatigue limit. A further study by Crews and Naik[3] concluded that the lateral support provided by the bolt clamp-up force influenced both the amount of hole elongation and the failure mode.

Shivakumar and Crews[4] used a two-dimensional finite element analysis to investigate the viscoelastic response of a simple bolted joint of graphite/epoxy laminates. An empirical equation was developed to calculate the clamp-up force as a function of time, material properties, and initial clamp-up force. The analysis predicted a clamp-up force relaxation of up to 31% after 20 years at room temperature/dry conditions. Slepetz et al.[5] investigated bolt clamp-up relaxation for highly clamped tension connectors for composite sandwich panels. Results indicated that the clamp-up force relaxation was not excessive at room temperature and below, but it was significant for higher temperatures near the service limit.

Methods for predicting the effect of bolt clamp-up force relaxation on the strength of mechanically fastened joints of thermoplastic composite materials were investigated during the present study. A test program, using two thermoplastic composite materials, was conducted to determine the influence of clamp-up force on joint strength, to measure the relaxation of the joint clamp-up force with time, and to measure the change of joint strength as a function of time.

Received Sept. 18, 1992; revision received July 25, 1993; accepted for publication Aug. 3, 1993.

*Associate Professor, Aerospace Engineering Department. Member AIAA.

†Structures Engineer, MS K22-04, P.O. Box 7730.

Test Description and Procedures

A two-phase test program was developed. The objective of the phase 1 testing was to establish a correlation between joint strength and fastener clamp-up force while the phase 2 tests were to quantify the short-time relaxation in the clamp-up force and to then measure the influence of relaxation on the joint strength.

Sixteen specimens of each of two composite materials, Dupont's IM6/KIII and ICI-Fiberite's IM8/APC(HTA), were tested during the phase 1 tests. A specimen of each material was tested for each of the possible combinations of two temperatures, two fastener types, and four torque levels. The two temperature conditions considered were room temperature (25.6°C)/dry and hot (121.1°C)/dry. Fastener types included both protruding head and countersink head titanium fasteners with nominal shank diameters of 0.635 cm. Torque levels of 0 (finger-tight), 3.39, 7.34, and 11.3 m-N were utilized to produce the desired range of clamp-up force.

Twelve specimens of each material were tested during the phase 2 tests. Both materials, the two fastener types, and the two temperature conditions were retained in the test array, but the number of torque levels was reduced to two (7.34 and 11.3 m-N) since the relaxation of the fastener clamp-up force would be more pronounced for the higher torque values. In addition, the time of duration of clamp-up force and in-plane tensile load were added as two new parameters. The 24 specimens of phase 2 were tested approximately 30 days after the application of the clamp-up force. Some of the specimens were also subjected to an in-plane axial tensile load to determine what effect in-service joint loading might have on the measured relaxation.

Each test coupon was a 32-ply quasi-isotropic laminate with a stacking sequence of $(45/90/-45/0)_{4s}$ and dimensions of 3.81×15.24 cm. A 0.635-cm-diam fastener hole was located 1.905 cm from each end of the coupon on the lengthwise centerline. Coupons prepared for the countersink fasteners had one of the two holes countersunk to a depth of 0.274 cm.

A single-shear joint was chosen for the test configuration since it permitted the use of both countersink and protruding head fas-

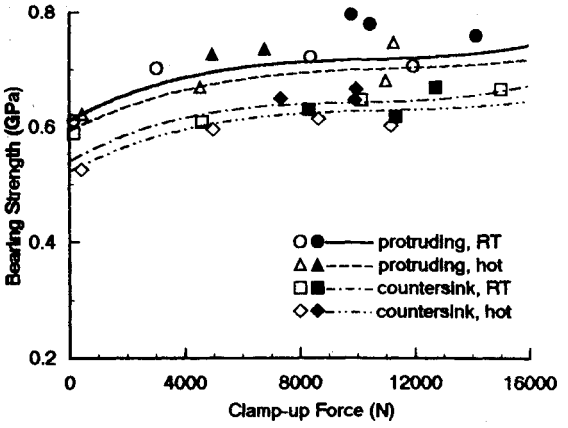

Fig. 1 Bearing strength vs clamp-up force for IM8/APC(HTA).

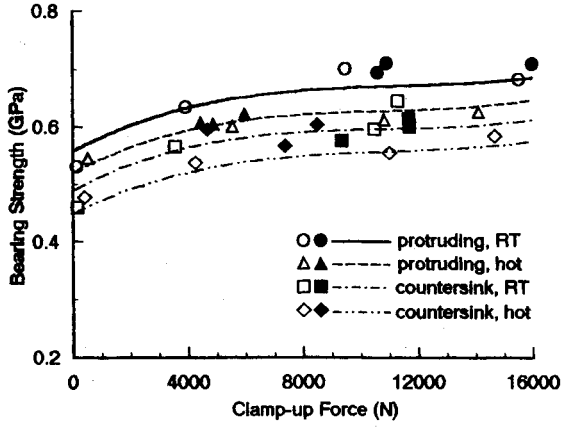

Fig. 2 Bearing strength vs clamp-up force for IM6/KIII.